

Structures and stabilities of Al_n^+ , Al_n , and Al_n^- ($n=13-34$) clusters

Andrés Aguado^{a)} and José M. López

Departamento de Física Teórica, Universidad de Valladolid, Valladolid 47011, Spain

(Received 24 October 2008; accepted 7 January 2009; published online 12 February 2009)

Putative global minima of neutral (Al_n) and singly charged (Al_n^+ and Al_n^-) aluminum clusters with $n=13-34$ have been located from first-principles density functional theory structural optimizations. The calculations include spin polarization and employ the generalized gradient approximation of Perdew, Burke, and Ernzerhof to describe exchange-correlation electronic effects. Our results show that icosahedral growth dominates the structures of aluminum clusters for $n=13-22$. For $n=23-34$, there is a strong competition between decahedral structures, relaxed fragments of a fcc crystalline lattice (some of them including stacking faults), and hexagonal prismatic structures. For such small cluster sizes, there is no evidence yet for a clear establishment of the fcc atomic packing prevalent in bulk aluminum. The global minimum structure for a given number of atoms depends significantly on the cluster charge for most cluster sizes. An explicit comparison is made with previous theoretical results in the range $n=13-30$: for $n=19, 22, 24, 25, 26, 29, 30$ we locate a lower energy structure than previously reported. Sizes $n=32, 33$ are studied here for the first time by an *ab initio* technique. © 2009 American Institute of Physics. [DOI: 10.1063/1.3075834]

I. INTRODUCTION

Structure is the most basic property of an atomic cluster. The detailed positioning of atoms determines the nuclear potential acting on the electrons. As such, cluster structure determines all other interesting properties, such as the response to radiation fields, the cluster reactivity, and the binding energy, to mention a few examples. It is then not surprising that intensive efforts have been devoted to elucidate the structure of clusters, both from theory and experiment. From the theoretical side, the complexity of the problem comes from the exponentially increasing number of local minima (structural isomers) on the potential energy surface (PES).¹ In order to solve this problem, several *unbiased* optimization methods have been developed, the most outstanding of which are the genetic² and basin hopping³ algorithms, although there are some others.⁴ These methods are highly efficient but also require an extensive sampling of the PES, so their conjoint use with an *ab initio* energy model is computationally problematic. The usual approach to overcome this problem is to apply first one of those unbiased methods to a simplified PES, such as that predicted by parametrized interaction models, and then reoptimize with an *ab initio* technique some of the candidate structures located in the unbiased search.⁵ From the experimental side, some cluster properties, such as the diffraction electron pattern,⁶ the photoelectron spectrum,⁷ or the cluster mobility within a drift cell,⁸ are measured and then compared to the results of theoretical predictions in order to make a structural assignment.

This paper is concerned with the theoretical determination of the structure of aluminum clusters with 13–34 atoms by employing an *ab initio* energy model. There are many previous studies on aluminum clusters due, on one hand, to the potential applications in microelectronics⁹ or nanocatalysis,¹⁰ and on the other hand, to basic interest in the

properties of simple metal clusters. We provide here a brief summary of the bibliography which is most relevant to the present work (for example, we do not mention many papers dealing with aluminum clusters with 2–12 atoms). Jarrold *et al.*¹¹ performed collision-induced dissociation experiments on Al_n^+ ($n=3-26$) and obtained enhanced cluster stabilities for Al_{13}^+ , Al_{13}^+ , Al_{14}^+ , and Al_{23}^+ . Taylor *et al.*¹² measured ultraviolet photoelectron spectra of Al_n^- with $n=3-32$ and found evidences of electron shell closings for sizes $n=13, 19$, and 23 . Both Ray *et al.*¹³ and King and Ross¹⁴ concluded that Al_{15}^+ has a very low stability and/or dissociation energy. Saito *et al.*¹⁵ reported mass spectra of bare Al_n^+ cluster ions and identified enhanced abundances for $n=14, 17, 20, 23$, and 28 . Hettich¹⁶ reported the corresponding mass spectra for Al_n^- anions, and large abundance drops were observed after $n=13, 20, 23$. Schriver *et al.*¹⁷ determined the ionization potentials (IPs) of Al_n clusters ($n < 80$) by photoionization spectroscopy and identified electron shell openings (particularly low IPs) at $n=14, 17, 23$, and 29 atoms. Jarrold and Bower¹⁸ determined the mobilities of Al_n^+ cluster ions, providing direct experimental information about the average shape of the clusters. Cha *et al.*¹⁹ measured photoelectron spectra of Al_n^- ($n=1-15$) clusters and found the spectrum of Al_{13}^- to be consistent with icosahedral symmetry. Li *et al.*²⁰ employed photoelectron spectroscopy of Al_n^- with n up to 162 atoms to corroborate the electron shell closings at 13, 19, and 23 atoms. More recently, Neal *et al.*²¹ measured the heat capacity curves for Al_n^+ cations with more than 16 atoms and found that the smallest cluster to show a well-defined melting transition is Al_{28}^+ , suggesting that some well-defined structural order might emerge at that cluster size.

On the theoretical side, there has been much activity regarding the correct global minima of aluminum clusters.²²⁻⁵² A controversy has arisen regarding the correct global minimum (GM) for Al_{13} : the optimizations based on parametrized potential models^{32,34,35,41,42,46,52} invariably

^{a)}Electronic mail: aguado@metodos.fam.cie.uva.es.

predict an icosahedral structure, but these methods do not contain an explicit description of the electronic degrees of freedom and their accuracy is questionable. A majority of the *ab initio* calculations [mostly based on density functional theory (DFT) and differing in the election of exchange-correlation functional, aluminum pseudopotential, and basis set] predict an icosahedron as the most stable structure,^{22–25,27,28,30,33,37,39,45} but a small number of calculations^{26,31,38,48,49} predict a decahedron to be more stable. In some cases the energy difference between icosahedral and decahedral structures is very small and therefore below the expected accuracy of DFT methods. Although no definite answer exists, it is worth pointing out that the icosahedron is 0.23 eV more stable than the decahedron in all-electron calculations performed with the Perdew–Burke–Ernzerhof (PBE) exchange-correlation functional⁵³ and a converged basis set.

We summarize now the most relevant attempts to optimize the structures of aluminum clusters with more than 13 atoms: Duque and Mañanes²⁵ calculated the geometric structures of aluminum clusters with up to 22 atoms using the local density approximation (LDA) within DFT. Akola *et al.*²⁹ obtained the atomic structures of aluminum cluster anions with 19, 20, and 23 atoms using the LDA and compared the theoretical electron density of states (DOS) to experimental photoelectron spectra. Aguado and López⁴⁴ determined the GM structures of Al_n^+ ($n=46–62$) using the PBE exchange-correlation functional within DFT. A preponderance of structures based on the bulk fcc atomic packing was observed, together with a strong preference to expose compact (111)-like surface facets. The obtained stabilities qualitatively correlated with the experimental latent heats obtained by Breaux *et al.*⁵⁴ Rao and Jena²⁶ and Fournier⁴⁸ gave the minimum energy geometric structures of Al_n , Al_n^- , and Al_n^+ with n up to 15 atoms employing the Becke–Perdew–Wang (BPW91) exchange-correlation functional. Neal *et al.*⁴⁷ located candidate global minima of Al_{31} and Al_{34} by selective quenching from high-temperature molecular dynamics (MD) simulations performed at the PBE/DFT level of theory. Chuang *et al.*⁴⁵ optimized the structures of neutral Al_n clusters with $n=2–23$, employing a genetic algorithm search on a tight-binding PES and further structural refinement at the LDA/DFT level of theory. Later on, Sun *et al.*⁵⁰ and Zhang *et al.*⁵¹ optimized the structures of neutral Al_n clusters with $n=19–30$, employing the same search method but with the final structural refinement performed at the PBE/DFT level of theory. Finally, Yao *et al.* published a couple of papers searching for the minimum energy structure of Al_{19} (Ref. 40) and Al_{20} (Ref. 43) using the full-potential linear muffin-tin-orbital MD method. These works provide an extensive data set to which we will compare our structural predictions.

Very recently, we determined the putative global minima of Al_n^+ ($n=34–83$) (Ref. 55) and Al_n^-/Al_n ($n=34–70$) (Ref. 56) at the PBE/DFT level of theory and compared the theoretical cohesive energies to experimental values, obtaining a good agreement for most sizes. The structures of the pure clusters were also employed to analyze the effect of substituting an aluminum atom by a copper impurity.⁵⁷ Distinct

groups of low-energy structures were identified in those studies: distorted decahedral fragments, which are the global minima for clusters with around 36 and 55 atoms; rounded “disordered” structures which are the global minima close to the electron shell closings (at 138 and 198 electrons) predicted by the spherical jellium model; and fragments of a fcc crystalline lattice which are the global minima for the rest of sizes. Many of the fcc structures contain stacking faults (SFs), as previously predicted by Manninen *et al.*³⁶ employing simpler energy models. Icosahedral isomers (favored by many parametrized aluminum potential models) were found to be high-energy isomers for all sizes. As the icosahedral isomers seem to be favored for aluminum clusters with around 13 atoms, we became interested in the following question: at which size do the icosahedral isomers become unstable? In order to close the gap between the small and large cluster sizes, we study here the structures adopted by aluminum clusters of an intermediate size, namely, $n=13–34$.

We close this introductory section by emphasizing the novel features of the present contribution: our work is the first one to consider, in a systematic way and at an *ab initio* level, the structures of both neutral, cation, and anion clusters in a broad size range, the upper size limit being 34 atoms. Most previous studies in this size range^{40,43,45,50,51} have considered only the neutral Al_n clusters, so the structures of cluster ions (more important from the experimental point of view) are considered here for the first time for most sizes (some exceptions are $n=13–15$, 19, 20, and 23).^{26,29,48} For many sizes (specifically, for $n=19$, 22, 24, 25, 26, 29, 30, 32, 33, 34), our GM structures have a lower energy than previously reported structures. In Sec. II we briefly present some technical details of the search method and of the theory level employed. Section III describes the cluster structures obtained in this work and compare them to previous theoretical results. Section IV shows a comparison with experimental results regarding cluster stability, structural, and electronic properties. Finally, Sec. V summarizes our main conclusions.

II. THEORY

Calculations were performed at the Kohn–Sham DFT (Ref. 58) level. We employ the SIESTA code,⁵⁹ with exchange and correlation effects treated within the spin-polarized generalized gradient approximation in its PBE implementation,⁵³ and norm-conserving pseudopotentials to describe the core electrons.^{60,61} The basis set employed to expand the cluster wave function contains five basis functions per Al atom (a double zeta plus polarization or DZP basis in standard notation⁵⁹). The spatial extension of the basis functions is determined by an energy shift⁵⁹ of 20 meV. The fast-Fourier-transform mesh employed to evaluate some terms in the Hamiltonian is determined by a mesh cutoff⁵⁹ of 100 Ry. The accuracy obtained by these settings was tested in our previous works,^{44,55} where we compared our results for the Al_2 dimer, small clusters, and bulk aluminum to experiment and previous calculations performed at different levels of theory (see the supplementary information in Ref. 44). A very recent

paper by Henry *et al.*⁶² independently demonstrated that PBE calculations performed with a DZP numerical basis set agree with the results of coupled cluster with single and double excitations (CCSD) calculations for Al clusters. Here we have further checked the convergence of the results with respect to basis set size by reoptimizing some cluster sizes using up to eight basis functions per Al atom [a triple zeta plus two polarization functions or TZP2 (Ref. 59) basis]. From this check we estimate the total energy differences between structural isomers to be converged up to 0.02 eV, which is within the expected accuracy of the PBE/DFT method. The DZP basis is therefore sufficient for this study. We also notice (see below) that the Al₁₃ icosahedron is more stable than the decahedron by 0.20 eV with the TZP2 basis set, which agrees almost perfectly with the value of 0.23 eV obtained in all-electron PBE calculations.^{27,33} This demonstrates the accuracy of our aluminum pseudopotential.

As in our previous works,^{55–57} the search for global minima was planned as a multistage task. In a first stage, we generated a sufficiently diverse set of initial structures for each cluster size. These structures are either taken directly from existing databases,⁶³ explicitly built by considering typical icosahedral, decahedral, and octahedral atomic packing, or obtained by quenching from finite temperature simulations performed with the same SIESTA code. These trial structures include, in particular, the global minima of different potential models not necessarily mimicking aluminum clusters. In this sense, we employ the system comparison approach advocated by Paz-Borbón *et al.*,⁶⁴ so that we do not rely on the accuracy of any potential model specifically designed for aluminum. This is especially important for Al clusters because, as previously mentioned,⁵⁵ present interatomic potentials do not describe well the structures of Al clusters. We also include explicitly in this first step the structures previously obtained by other authors. In a second stage, all those structures are fully optimized with the SIESTA code. Some of the isomers can be excluded from further consideration at the end of this stage due to their very high energy. In a last and most computationally expensive stage, we take the five to ten more stable structures for each size and consider them as seeds for further refinement. From each cluster of size n , we build $n+m$ and $n-m$ clusters (with $m=1-5$) by adding or removing atoms from its surface in many different ways. Each time we identify a better minimum for a given cluster size, it is considered the seed for a new refinement cycle, which is stopped only when we repeatedly reobtain the same structures. The procedure is possibly as systematic as it can be without the explicit employment of unbiased algorithms, and the number of different isomers tried for each size is at least 100 (except for the smallest sizes $n=13-15$). The success of this “manual” search strategy has been demonstrated for larger clusters by the good agreement between the experimental and theoretical cohesive energies.^{55,56} We expect it to be even more reliable for the smaller cluster sizes considered here, as the number of local minima on the PES is correspondingly reduced. In fact, a direct demonstration of the reliability of our search method is the fact that we find better global minima than previously reported for $n=19, 22, 24, 25, 26, 29, 30, 32, 33, 34$.

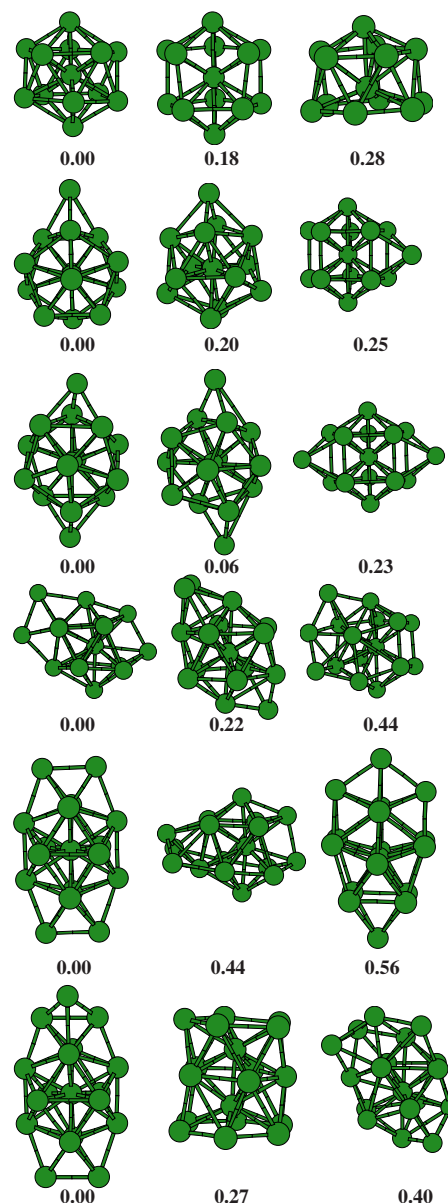


FIG. 1. (Color online) GM structures and some low-lying isomers of neutral Al_{*n*} clusters with $n=13-18$. The numbers below the isomers give the total energy differences (in eV) with respect to the GM, and cluster sizes increase from top to bottom.

III. CLUSTER STRUCTURES: COMPARISON TO PREVIOUS THEORETICAL RESULTS

A. Clusters with $n=13-18$ atoms

Figure 1 shows our calculated GM structures for neutral Al_{*n*} ($n=13-18$) clusters. In this and the following figures, we do not show exactly the lowest-energy isomers, but instead a representative selection of different structures. This means that for almost all sizes, there are several isomers with higher binding energies than those explicitly shown in the figures. For $n=13$ we obtain a Jahn–Teller distorted icosahedron as the GM (the point group symmetry is lowered from I_h to D_{3d}), while a distorted decahedron is 0.18 eV higher in total energy with the DZP basis set. As mentioned above, this energy difference increases to 0.20 eV when the TZP2 basis is used instead, which agrees well with the energy difference

of 0.23 eV found in all-electron PBE calculations.^{27,33} The next isomer will be discussed below, as it is found to be the GM for Al_{13}^+ .

The GM structure of Al_{14} is obtained by capping one of the triangular faces of the 13-atom icosahedron and has C_{3v} symmetry. The next isomer is obtained by capping instead one of the edges of the icosahedron: the underlying icosahedral structure is distorted to provide four bonds between Al_{13} and the capping atom. Capping one of the square faces of the 13-atom decahedron leads to another high-energy isomer.

The GM of Al_{15} results from capping two diametrically opposed triangular faces of the 13-atom icosahedron, which leads a prolate structure with only C_s symmetry due to the Jahn–Teller distortion. Again, capping two opposite edges of the 13-atom icosahedron or two noncontiguous square faces of the 13-atom decahedron results in high-energy isomers.

Additional capping of the 13-atom icosahedron leads the GM of Al_{16-18} . Al_{16} is obtained by adding a new Al atom close to one of the capping atoms of Al_{15} . The structure is quite distorted but preserves the C_s point group symmetry. Al_{17} recovers a higher symmetry (C_{2h} or D_{2h} depending on the accuracy required from the atomic positions when determining the point group) and a more prolate shape, as a result of capping with 2 Al atoms on different sides of the 13-atom icosahedron. Al_{18} shows an intriguing structure of C_s symmetry, where the additional atom is not capping the 13-atom icosahedron but prefers to sit on the next atomic shell with a low coordination. This demonstrates a strong preference for this size to adopt a structure as prolate as possible even at the expense of a poor atomic packing. For $n=16-18$, the low-energy isomers are typically found by capping the 13-atom icosahedron in many different ways. The best decahedral isomer for Al_{17} , for example, is already 0.56 eV higher than the GM. We also notice the presence of a low-energy isomer of Al_{18} , which shows an atomic stacking sequence of 5–1–5–1–6, and which will form the basis for the GM of Al_{20} .

Our results for Al_n^+ ($n=13-15$) differ substantially from those of Rao and Jena²⁶ and Fournier,⁴⁸ who obtained instead decahedral structures but employing a different (BPW91) exchange-correlation functional. Later on, Rao and Jena²⁷ and Khanna *et al.*³³ confirmed that icosahedral structures are more stable in all-electron PBE calculations, in good agreement with our results. Moreover, our GM structures for $n=13-18$ are exactly the same as those found by Chuang *et al.*⁴⁵ using the LDA approximation.

Much less is known about the structures of aluminum cluster ions in the range $n=13-18$. Figure 2 shows our calculated GM structures for Al_n^+ and Al_n^- only when they differ significantly from the corresponding neutral geometries. Al_{13}^- (not shown) adopts a perfect icosahedral structure with I_h symmetry, so it does not support the Jahn–Teller distortions observed in the neutral cluster. Al_{13}^- has exactly 40 valence electrons and therefore (see below) is a spherical electron shell closing. An explicit comparison of the electron DOS to experimental photoelectron spectra⁶⁵ shows that only the DOS of the icosahedral isomer is able to match the experimental spectrum. Al_{13}^+ adopts a completely different and

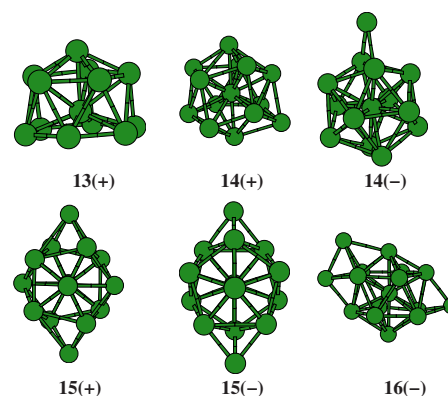


FIG. 2. (Color online) GM structures of Al_n^+ and Al_n^- cluster ions with $n=13-18$. Only those structures which substantially differ from the corresponding Al_n geometries are shown. Below each structure, we give the number of atoms and the cluster charge.

more open structure, with C_s symmetry and an atomic stacking sequence of 1–5–1–6 (as opposed to the 1–5–1–5–1 typical of the icosahedron).

In Al_{14}^- , the additional atom is capping one edge of the 13-atom icosahedron, which gives a C_s symmetry. Compared to the corresponding isomer of Al_{14} (see Fig. 1), the underlying Al_{13}^- hardly distorts and therefore the capping atom is coordinated to only two atoms. Al_{14}^+ is obtained by capping the Al_{13}^+ cluster to provide a 1–5–1–6–1 stacking sequence.

For $n=15$ there are only minor modifications with respect to the neutral cluster structure. For the anion, the distortion of the underlying 13-atom icosahedron is again removed, which increases the symmetry from C_s to D_{3d} . For the cation, on the contrary, the two adatoms distort the 13-atom icosahedron much more so that each adatom is coordinated to four Al atoms (as compared to only three bonds in the neutral and the anion). Finally, the structure of Al_{16}^- is shown just to emphasize again the higher stability of the 13-atom icosahedron: the adatom on the right side does not deform the icosahedron and is coordinated to only three Al atoms instead of four in the neutral and the cation.

In summary, we observe a very high stability of the 13-atom icosahedral building block for cluster anions. This stability is progressively reduced when passing first to the neutrals and then to the cations, for which the icosahedral structure is not even the GM for $n=13$. This trend is attenuated with increasing size so that all charge states share the same GM for $n=17, 18$. Our GM structures for $n=13-15$ agree with those given by Fournier⁴⁸ only for the cations and are different for the anions.

B. Clusters with $n=18-34$ atoms

Within this size range, we have found some previously unreported global minima. Figure 3 shows the global minima and some structural isomers for sizes $n=19-22$. The GM structure of Al_{19} and Al_{19}^- is formed by a 14-atom building block with 1–5–1–6–1 stacking sequence (the GM for Al_{14}^+) plus five adatoms in a “belt” arrangement, giving a C_1 point group symmetry. This structure has not been reported previously. Yao *et al.*⁴⁰ reported a similar structure for Al_{19} but differing in the detailed positioning of the five adatoms. The

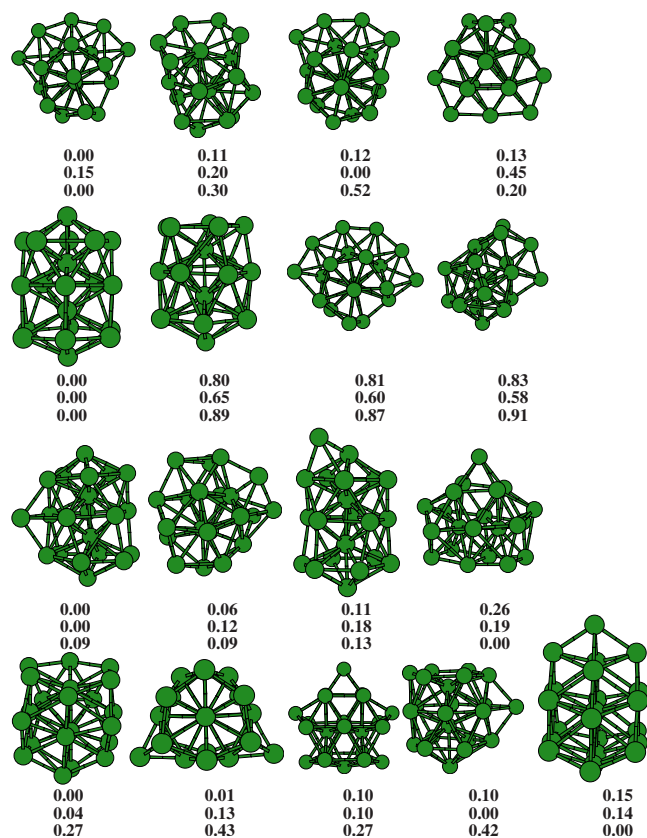


FIG. 3. (Color online) GM structures of aluminum clusters with $n=19-22$. Cluster sizes increase from top to bottom, and the numbers below the isomers give the total energy differences (in eV) with respect to the GM. Top row: neutral Al_n clusters; intermediate row: Al_n^+ cations; and bottom row: Al_n^- anions.

GM reported by Sun *et al.*,⁵⁰ namely, a hexagonal prism with four adatoms, is 0.12 eV higher in energy for Al_{19} according to our calculations, but precisely that structure is our GM for Al_{19}^+ . The well known double icosahedron predicted to be the GM by most empirical potential models⁵² has a much higher energy according to the Kohn–Sham results.

The GM for $n=20$ is the same for all charge states, with the atoms arranged according to the 1–5–1–5–1–6–1 stacking sequence. This structure, of C_s symmetry, has been obtained in previous works.^{29,43,45,50} The GM structure of Al_{21} and Al_{21}^+ is obtained by adding one atom to Al_{20} in the equatorial position and has C_1 symmetry. This structure has also been found previously.^{45,50} Al_{21}^- adopts, on the contrary, a very different structure with a higher (C_2) rotational symmetry.

For $n=22$ atoms, the GM structures are different for each charge state. Neutral Al_{22} adopts a quite disordered geometry with C_1 symmetry, although it is degenerate with another structure obtained by removing one Al atom from the Al_{23} GM (see below). Al_{22}^+ adopts an interesting structure which demonstrates the tendency of Al clusters to form hexagonal rings (as opposed to the pentagonal rings typical of icosahedra) within this size range. It consists of a 21-atom building block with 1–6–1–6–1–6 stacking sequence plus one equatorial adatom, giving a C_s symmetry. Finally, Al_{22}^- adopts for the first time a structure resembling the bulk fcc symmetry. It has a high D_{3h} symmetry and is formed by stacking three planes of atoms with a SF in between. This

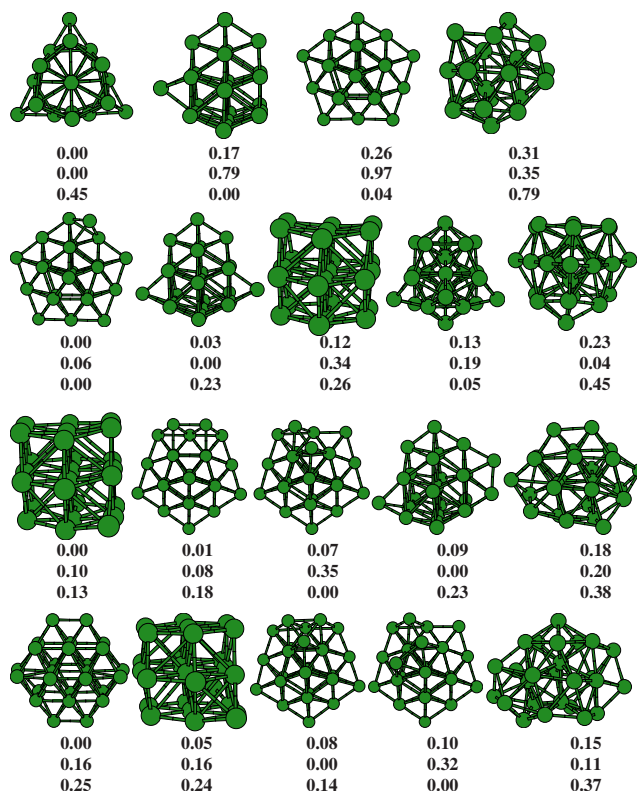


FIG. 4. (Color online) GM structures of aluminum clusters with $n=23-26$. The rest of the caption is the same as in Fig. 3.

structure resembles the “stacking-fault” structures observed in our previous works on larger Al clusters.^{55,56} None of these three structures has been previously reported: the structure obtained by Sun *et al.*⁵⁰ is 0.10 eV above our GM for Al_{22} .

Figure 4 shows the relevant structures in the size range $n=23-26$. The GM of Al_{23} and Al_{23}^+ coincides with the one obtained by Sun *et al.*⁵⁰ It has a high C_{3v} symmetry and consists of a hexagonal prism (6–1–6–1–6 stacking sequence) plus three adatoms decorating the equatorial region. The GM of Al_{23}^- is instead obtained by capping Al_{22}^- , giving a structure with C_s symmetry. A perfect decahedron, suggested by Kumar *et al.*²⁸ to be the GM for neutral Al_{23} , is also especially stable as an anion, so both isomers should coexist under typical experimental conditions.

We obtain several competing structures for $n=24$. From left to right in Fig. 4, these are a perfect 23-atom decahedron plus one adatom (C_1 symmetry), a C_{2v} isomer obtained by capping two opposite facets of the Al_{22}^- GM structure, a C_2 structure which is the basis for the GM structure of Al_{25} (see below), a 19-atom double icosahedron capped with five atoms, and a C_s isomer which is the GM predicted by Sun *et al.*⁵⁰ for neutral Al_{24} . Depending on the charge state, two or three of these isomers are degenerate in energy. A similar high degeneracy is observed for $n=25$, involving again decahedral structures and fcc fragments with SFs as building blocks to which adatoms are added in different ways, leading always to GM structures with C_1 rotational symmetry. For $n=26$, both cation and anion structures are obtained by capping the 23-atom decahedron. The capping is more symmetrical for the cation which leads to a C_s point group. For

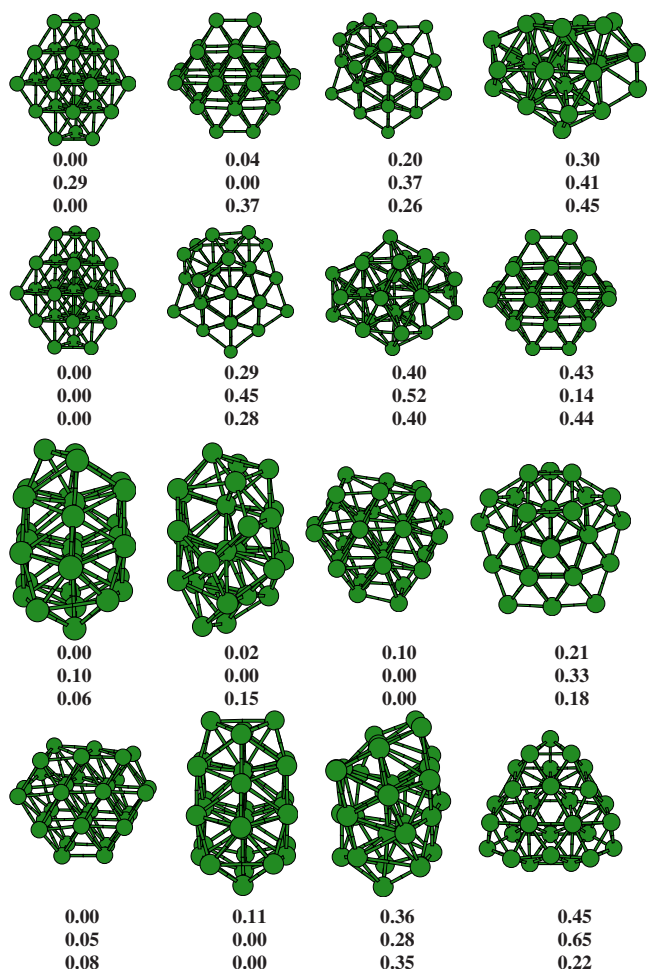


FIG. 5. (Color online) GM structures of aluminum clusters with $n=27-30$. The rest of the caption is the same as in Fig. 3.

neutral Al_{26} , a fcc fragment with C_{2v} symmetry is preferred instead. All the global minima for $n=24-26$ are reported here for the first time, to the best of our knowledge.

We proceed to describe the structure of clusters with $n=27-30$ atoms (see Fig. 5). A recent report by Zhang *et al.*⁵¹ claimed that double-tetrahedron structures are favored in this size range for neutral clusters. A perfect double-tetrahedron would be obtained with 30 atoms and consists of two 20-atom tetrahedra sharing one basal plane. In fact, such a structure would pertain to the “SF family” using the nomenclature of our previous works on larger clusters:^{55,56} the plane shared by the two tetrahedra changes locally the stacking sequence from fcc to hcp-like.

Our search results agree with those of Zhang *et al.*⁵¹ only for $n=27$ and $n=28$. For $n=28$, the GM structure is the same for all charge states and is obtained by removing the two vertex atoms from a perfect 30-atom double tetrahedron, which gives a D_{3h} symmetry. Those atoms have a very low coordination and their removal seems to be energetically favorable. Removing one more atom from the basal plane shared by the two tetrahedra lowers the symmetry from D_{3h} to C_{2v} and leads to the GM structure of Al_{27} and Al_{27}^+ . However the GM structure of Al_{27} is nearly degenerate with a fcc isomer of C_s symmetry obtained by adding one atom to the Al_{26} GM structure. The fcc isomer is in fact the GM for Al_{27}^+ .

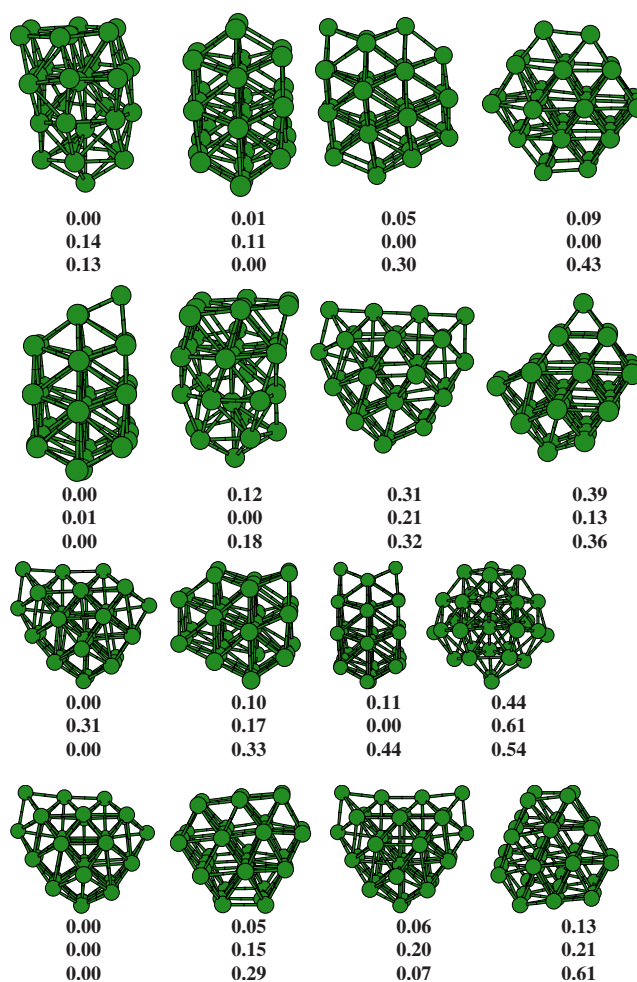


FIG. 6. (Color online) GM structures of aluminum clusters with $n=31-34$. The rest of the caption is the same as in Fig. 3.

In this size range, the stability of the isomers obtained by capping the 23-atom decahedron is reduced. We speculate that the highly symmetric and compact structure of Al_{28}^+ , with perfect (111)-like surface facets, is responsible for the emergence of a well-defined melting peak at this size.²¹

According to our calculations, double-tetrahedral isomers have energies more than 0.5 eV higher than the true global minima for $n=29-30$ and therefore are not competitive isomers anymore. Instead we obtain a number of nearly degenerate isomers with low symmetry, some of them based on a mixture of icosahedral and fcc packing while others (for example, Al_{30}) are distorted fragments of a fcc lattice. The GM structure of Al_{30}^+ and Al_{30}^- has at least a mirror plane and therefore C_s point group symmetry.

Finally, we show in Fig. 6 the putative global minima for $n=31-34$. For Al_{31} we predict the same GM structure as Neal *et al.*,⁴⁷ although there are again many nearly degenerate isomers, and the GM structures of charged clusters are not the same. The structure of Al_{31} is a mixture of icosahedral (lower part of the cluster in the orientation given in Fig. 6) and fcc (upper part) packing, while the charged clusters adopt SF structures. These two types of structures compete also for $n=32$.

For $n=33, 34$ we observe for the first time the emergence of the distorted decahedral fragments discussed in our

previous works, and which are the GM structures for sizes around 36 and 55 atoms.^{55,56} Except for Al_{33}^+ , which adopts a SF structure with C_{2v} point group, these structures are obtained by removing atoms from the perfect distorted decahedral structure of Al_{36} . All the GM structures will be made freely available to other researchers through the web.⁶⁶

We close this section with a more general comparison of our results to those published by Sun *et al.*⁵⁰ and Zhang *et al.*⁵¹ These authors emphasized the strong structural preference of Al clusters to expose compact, (111)-like, surface facets. Our results support that general observation, which had been previously remarked.⁴⁴ However, our results do not support other general observations. For example, Sun *et al.*⁵⁰ claimed that the lowest-energy structure has always more symmetry than the high-energy isomers, while many of our global minima have no rotational symmetry at all (C_1 point group) and can be considered to be a mixture of different packing motifs. A well-defined symmetry is to be expected only for much larger clusters. Also, many of the GM structures of the larger clusters^{55,56} cannot be explained in terms of the growth motifs advanced in Refs. 50 and 51 (for example, the distorted decahedral isomers). Sun *et al.*⁵⁰ also found that the GM structures of Al_n and Al_n^- clusters are the same with the only exception of $n=19$ and rationalized this finding by saying that these clusters are already sufficiently big to not be affected by the charge state.⁵⁰ Our calculations show exactly the opposite trend: the GM structure depends significantly on the charge state for many sizes. In fact, our previous works^{55,56} have shown that the GM structures of cations and anions may be different even for sizes as big as 70 atoms. Once more, cation and anion structures are expected to be the same only for much larger sizes. In this regard, we stress that it is very important to treat Al_n , Al_n^+ , and Al_n^- as *independent* optimization problems: for example, optimizing first the neutrals and then using a few neutral structures to reoptimize the structures of cluster ions will frequently lead to missing the correct GM of the charged clusters.

IV. CLUSTER STABILITY AND OTHER STRUCTURAL AND ELECTRONIC PROPERTIES: COMPARISON TO EXPERIMENT

As typical measures of cluster stability we show in Fig. 7 the cohesive energy (the total binding energy of the cluster divided by the number of atoms) and the second energy difference defined as $\Delta_2(n) = E(n+1) + E(n-1) - 2E(n)$, where $E(n)$ is the total energy of the n -atom cluster. A cluster size n which is especially stable (with respect to its neighboring cluster sizes) is called a magic number. It will appear as a marked maximum in the $\Delta_2(n)$ plot and either as a local maximum or as a point with negative curvature in the cohesive energy plot. According to Fig. 7, our calculations predict the following magic numbers (in parentheses we show those magic numbers of secondary importance): $n=14, 20, 28, (30), 32$ for neutral Al_n clusters, with Al_{20} having the highest stability; $n=14, 17, (20), 23, (28), (31)$ for the cations, with the highest stability occurring at Al_{23}^+ ; and $n=13, 17, 20, 23, 27, (31)$ along the anion series. The predicted magic numbers are in very good agreement with the experimental abun-

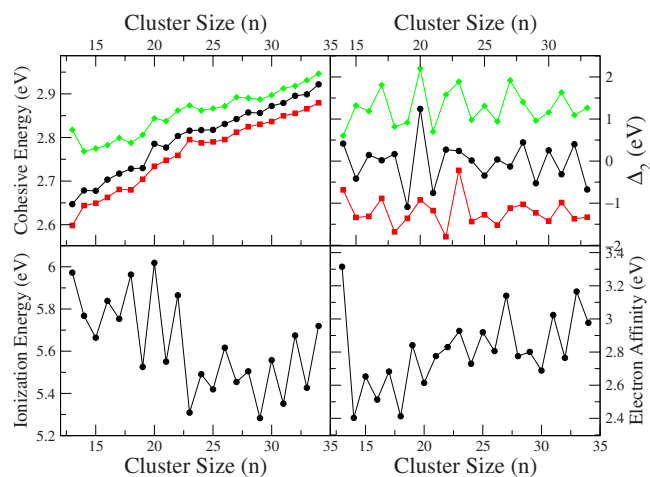


FIG. 7. (Color online) The top panel shows the cohesive energies (left side) and second energy differences (right side) for Al_n (black points), Al_n^+ (red squares), and Al_n^- (green diamonds) clusters. The results for cations and anions have been vertically shifted in order to help visualization. The bottom panel shows the adiabatic IEs (left side) and adiabatic EAs (right side); see text for a definition of these quantities.

dances observed in mass spectra, both for cations¹⁵ and anions.¹⁶ Our results also confirm the enhanced stabilities of Al_n^+ predicted by Jarrold and co-workers^{11,13} on the basis of collision-induced dissociation experiments. We therefore expect the predicted stabilities to be reliable also for neutral clusters.

As measures of electronic stability, we show in Fig. 7 the adiabatic ionization energy $\text{IE}(n) = E[\text{Al}_n^+] - E[\text{Al}_n]$ and the adiabatic electron affinity $\text{EA}(n) = E[\text{Al}_n] - E[\text{Al}_n^-]$ of the neutral clusters, where all energies refer to the corresponding global minima. We have also calculated the corresponding vertical IE and EA (not shown explicitly), which are the energies required to remove or add one electron without allowing for structural relaxation. A large IE value indicates a high electronic stability, and a large drop in the IE is usually associated with the opening of a new electron shell (this last assertion has to be taken with some caution in the case of aluminum clusters, as adding one atom introduces three additional valence electrons. A very low IE value can be taken as an indication that the corresponding cation is an electron shell closing). However, for the small clusters considered here, the odd-even oscillations are so strong that they partly mask the electron shell closings. Especially large IE values are obtained for sizes $n=13, 18, 20, 22$, and a shell opening is only seen clearly for Al_{23} . Our IE curve reasonably reproduces the photoionization results of Schriver *et al.*¹⁷ regarding the location of the maxima and the size of the odd-even effect. Clusters with an especially low EA (sizes $n=14$ and 18) also have an enhanced electron stability, while very large EA values (sizes $n=13$ and 27) signal the proximity of an electron shell closing. We therefore find Al_{13}^+ , Al_{23}^+ , and Al_{27}^- to be marked electron shell closings (these are confirmed also by an examination of the corresponding vertical excitation processes).

Jarrold and Bower¹⁸ measured the mobilities and collision cross sections of Al_n^+ clusters using drift tube techniques. Unlike clusters with covalent⁶⁷ or ionic^{68,69} bonding,

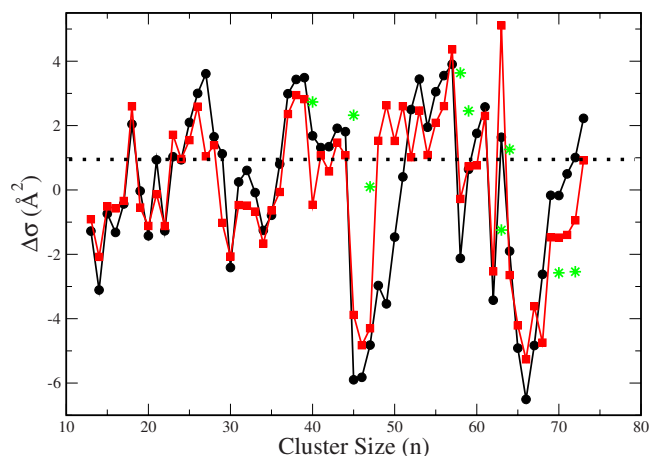


FIG. 8. (Color online) The filled black points show the deviation $\Delta\sigma$ of the experimental collision cross sections of Al_n^+ cluster ions ($n=13-73$) from the average behavior obtained through a power-law regression $\sigma(n)=An^B$. The results of the regression are $A=24.971$ and $B=0.519\,03$, when the cross sections are expressed in \AA^2 . Filled red squares show the corresponding theoretical results, for which the regression parameters are $A=19.076$ and $B=0.5645$. For some sizes, there are two nearly degenerate isomers which have significantly different collision cross sections, and both are candidate global minima according to the expected DFT accuracy. The green stars show the $\Delta\sigma$ values for the nearly degenerate isomers.

which have strongly directional bonding properties, the mobilities of simple metal clusters are not expected to show large fluctuations with size. We have determined the cation collision cross sections $\sigma(n)$ using the MOBCAL code.⁷⁰ The cross sections (not shown explicitly) systematically increase with the number of atoms n , which makes it difficult to visualize their size dependence. We therefore have fitted a power-law expression to the theoretical cross sections and plotted in Fig. 8 the deviation $\Delta\sigma(n)$ with respect to such average behavior. This helps to magnify the size fluctuations of the collision cross sections of Al clusters so that a meaningful analysis can be performed. Plotting $\Delta\sigma(n)$ also eliminates a systematic error: the theoretical σ values are, on average, about 10% smaller than the corresponding experimental values. We are mostly interested in the size-dependent fluctuations and not on the absolute values of the cross sections, which may depend both on experimental parameters such as sample temperature (the theoretical cross sections correspond to the structures at 0 K, while the experiments are performed at finite temperature), on approximations of the methods employed to derive the cross sections,⁷⁰ or on the accuracy with which DFT predicts the correct bond lengths. As the collision cross sections were not calculated in our previous paper on larger clusters,⁵⁵ we include here results for sizes $n=13-73$. Globally, the size dependence of $\Delta\sigma$ is in very good agreement with the experimental measurements. Specifically, there are marked local minima for $n=14, 20, 22, 30, 34, 46, 58, 62$, and 66 ; the collision cross section is especially large for $n=18, 26, 36-39, 57, 61$, and 63 . Deviations from the experimental trend appear for $n=27$ and $n=48-52$, which suggests that our global minima may not be the same as the ones in the experimental beam for those sizes. For some sizes, there are isomers nearly degenerate with the global minima, the energy difference being smaller than 5 meV/atom. If the collision cross sections of

those isomers are sufficiently different, they are plotted separately with stars in Fig. 8. The collision cross sections are influenced by both structural and electronic effects: on one hand, a spherical cluster is expected to have a lower σ than an ellipsoidally deformed cluster. This explains the minima for Al_{14}^+ , Al_{46}^+ , and Al_{66}^+ , for example; on the other hand, a closed electronic configuration usually induces shorter and stiffer bonds as compared to clusters with an open electron shell, partially contributing to the rest of minima. Al_{18}^+ has both a strong prolate deformation and an open electronic shell, and its collision cross section is therefore a marked local maximum. The rest of features can be similarly explained.

In our previous works on larger clusters,^{55,56} we found that the magic numbers in the stability curve result from a complex interplay between electronic and structural effects. We find that the same is true for the small clusters. Each magic size would deserve a separate explanation, but we just provide a few examples here. Along the neutral series, the most prominent magic number is Al_{20} . It has a more compact structure (its mobility is also a local maximum, as in Fig. 8 for the cations) than Al_{19} and Al_{21} and it can be considered a geometrical shell closing because it does not have any “adatom” with low coordination. Moreover, its IE is the highest, so this cluster is both structurally and electronically stable, hence its remarkable stability. The structural effect is sufficiently important that Al_{20}^+ and Al_{20}^- adopt the same structure and are also magic numbers, although not so strong as in the neutral series because they do not have a high electron stability. Other clusters with both structural and electronic stability are Al_{13}^+ , Al_{23}^+ , Al_{23}^- , and Al_{28} . Al_{23} has a very low IE because Al_{23}^+ is an electron shell closing, so its stability is not especially high even if it has the same highly symmetric GM as the cation. The EA of Al_{23} is a local maximum which points to a high electronic stability for Al_{23}^- . In fact, the vertical IE of Al_{23}^- (not shown) is a marked maximum. Al_{23}^- has two nearly degenerate isomers as possible global minima, one of which is a perfect 23-atom decahedron, that is, a geometric shell closing. Most other magic numbers can be similarly interpreted, with the relative contributions of electron and structural stabilities varying for each particular case.

V. CONCLUSIONS

In summary, we have obtained putative GM structures for both neutral Al_n and singly charged Al_n^+ and Al_n^- clusters ($n=13-34$) using a first-principles methodology based on DFT. We have provided a careful and critical comparison to previous theoretical determinations of cluster structure. Our global minima search locates lower energy isomers than previously reported for sizes $n=19, 22, 24, 25, 26, 29, 30, 32, 33, 34$. We also compare favorably our results to experimental determinations of cluster structure, stability, and electronic properties. Together with our previous research on larger clusters,^{44,55-57} our work provides a consistent description of the structural size evolution of Al clusters with 13 to about 80 atoms. Only the smallest clusters ($n=13-21$) adopt structures based on icosahedral motifs. For larger clusters, a competition between bulklike fcc, decahedral, and disor-

dered structures is seen. Even if some small clusters such as $n=27-28$ adopt fcc-like structures, the bulk symmetry cannot be considered to be fully established until at least $n \approx 70$, and possibly some exceptions will remain even for larger sizes. Moreover, our previous works have shown that the fcc-like structures contain a significant proportion of SFs, that is, regions with local hcp-like atomic packing. The rich structural diversity of Al clusters comes from an interplay between structural and electronic effects, which presently is not properly captured by any parametrized potential model of atomic interactions. Even quite elaborate models such as ReaxFF (Ref. 52) continue to predict icosahedral global minima up to 55 atoms and substantial remnants of icosahedral ordering for clusters with up to 512 atoms. ReaxFF is able to reproduce the tendency (previously observed in *ab initio* calculations)^{44,55-57} of Al clusters to form mixed fcc/hcp structures, but only at larger cluster sizes. In summary, developing a reliable interatomic potential for Al clusters of small and intermediate size still remains a significant challenge.

ACKNOWLEDGMENTS

We would like to thank Professor Martin F. Jarrold for providing us with the experimental collision cross sections for Al_n^+ clusters shown in Fig. 8. We gratefully acknowledge the support of “Ministerio de Ciencia e Innovación,” the European Regional Development Fund, and “Junta de Castilla y León” (Project Nos. FIS2008-02490/FIS and GR120).

¹ *Energy Landscapes*, by D. J. Wales (Cambridge University Press, Cambridge, 2003).

² R. L. Johnston, *Dalton Trans.* **2003**, 4193.

³ D. J. Wales and J. P. K. Doye, *J. Phys. Chem. A* **101**, 5111 (1997).

⁴ Y. Wang, J. Zhuang, and X. Ning, *Phys. Rev. E* **78**, 026708 (2008).

⁵ R. Ferrando, A. Fortunelli, and R. L. Johnston, *Phys. Chem. Chem. Phys.* **10**, 640 (2008).

⁶ D. Schooss, M. N. Blom, J. H. Parks, B. von Issendorff, H. Haberland, and M. M. Kappes, *Nano Lett.* **5**, 1972 (2005).

⁷ O. Kostko, B. Huber, M. Moseler, and B. von Issendorff, *Phys. Rev. Lett.* **98**, 043401 (2007).

⁸ A. A. Shvartsburg, R. R. Hudgins, P. Dugourd, and M. F. Jarrold, *Chem. Soc. Rev.* **30**, 26 (2001).

⁹ A. O. Orlov, I. Amlani, G. H. Bernstein, C. S. Lent, and G. L. Snider, *Science* **277**, 928 (1997).

¹⁰ M. Valden, X. Lai, and D. W. Goodman, *Science* **281**, 1647 (1998).

¹¹ M. F. Jarrold, J. E. Bower, and J. S. Kraus, *J. Chem. Phys.* **86**, 3876 (1987).

¹² K. J. Taylor, C. L. Pettiette, M. J. Craycraft, O. Cheshnovsky, and R. E. Smalley, *Chem. Phys. Lett.* **152**, 347 (1988).

¹³ U. Ray, M. F. Jarrold, J. E. Bower, and J. S. Kraus, *J. Chem. Phys.* **91**, 2912 (1989).

¹⁴ F. L. King and M. M. Ross, *Chem. Phys. Lett.* **164**, 131 (1989).

¹⁵ Y. Saito, I. Katakuse, and H. Ito, *Chem. Phys. Lett.* **161**, 332 (1989).

¹⁶ R. L. Hettich, *J. Am. Chem. Soc.* **111**, 8582 (1989).

¹⁷ K. E. Schriver, J. L. Persson, E. C. Honea, and R. L. Whetten, *Phys. Rev. Lett.* **64**, 2539 (1990).

¹⁸ M. F. Jarrold and J. E. Bower, *J. Chem. Phys.* **98**, 2399 (1993).

¹⁹ C. Cha, G. Ganteför, and W. Eberhardt, *J. Chem. Phys.* **100**, 995 (1994).

²⁰ X. Li, H. Wu, X. Wang, and L. Wang, *Phys. Rev. Lett.* **81**, 1909 (1998).

²¹ C. M. Neal, A. K. Starace, and M. F. Jarrold, *Phys. Rev. B* **76**, 054113 (2007).

²² U. Rothlisberger, W. Andreoni, and P. Gianozzi, *J. Chem. Phys.* **96**, 1248 (1992).

²³ V. Kumar, *Phys. Rev. B* **57**, 8827 (1998).

²⁴ J. Akola, H. Häkkinen, and M. Manninen, *Phys. Rev. B* **58**, 3601 (1998).

²⁵ F. Duque and A. Mañanes, *Eur. Phys. J. D* **9**, 223 (1999).

²⁶ B. K. Rao and P. Jena, *J. Chem. Phys.* **111**, 1890 (1999).

²⁷ B. R. Rao, S. N. Khanna, and P. Jena, *Phys. Rev. B* **62**, 4666 (2000).

²⁸ V. Kumar, S. Bhattacharjee, and Y. Kawazoe, *Phys. Rev. B* **61**, 8541 (2000).

²⁹ J. Akola, M. Manninen, H. Häkkinen, U. Landman, X. Li, and L. Wang, *Phys. Rev. B* **62**, 13216 (2000).

³⁰ J. Akola and M. Manninen, *Phys. Rev. B* **63**, 193410 (2001).

³¹ R. R. Zope and T. Baruah, *Phys. Rev. A* **64**, 053202 (2001).

³² L. D. Lloyd, R. L. Johnston, C. Roberts, and T. Mortimer-Jones, *ChemPhysChem* **3**, 408 (2002).

³³ S. N. Khanna, B. K. Rao, and P. Jena, *Phys. Rev. B* **65**, 125105 (2002).

³⁴ J. Joswig and M. Springborg, *Phys. Rev. B* **68**, 085408 (2003).

³⁵ J. P. K. Doye, *J. Chem. Phys.* **119**, 1136 (2003).

³⁶ K. Manninen, J. Akola, and M. Manninen, *Phys. Rev. B* **68**, 235412 (2003).

³⁷ A. Mañanes, F. Duque, F. Méndez, M. J. López, and J. A. Alonso, *J. Chem. Phys.* **119**, 5128 (2003).

³⁸ M. D. Deshpande, D. G. Kanhere, I. Vasiliev, and R. M. Martin, *Phys. Rev. B* **68**, 035428 (2003).

³⁹ R. Pushpa, S. Narasimhan, and U. Waghmare, *J. Chem. Phys.* **121**, 5211 (2004).

⁴⁰ C. Yao, B. Song, and P. Cao, *Phys. Rev. B* **70**, 195431 (2004).

⁴¹ R. Werner, *Eur. Phys. J. B* **43**, 47 (2005).

⁴² A. Sebetci and Z. B. Güvenc, *Modell. Simul. Mater. Sci. Eng.* **13**, 683 (2005).

⁴³ C. Yao, B. Song, and P. Cao, *Phys. Lett. A* **341**, 177 (2005).

⁴⁴ A. Aguado and J. M. López, *J. Phys. Chem. B* **110**, 14020 (2006).

⁴⁵ F. Chuang, C. Z. Wang, and K. M. Ho, *Phys. Rev. B* **73**, 125431 (2006); see also **77**, 079904 (2008).

⁴⁶ W. Zhang, F. S. Zhang, and Z. Y. Chu, *Eur. Phys. J. D* **43**, 97 (2007).

⁴⁷ C. M. Neal, A. K. Starace, M. F. Jarrold, K. Joshi, S. Krishnamurty, and D. G. Kanhere, *J. Phys. Chem. C* **111**, 17788 (2007).

⁴⁸ R. Fournier, *J. Chem. Theory Comput.* **3**, 921 (2007).

⁴⁹ Y. Sun, M. Zhang, and R. Fournier, *Phys. Rev. B* **77**, 075435 (2008).

⁵⁰ J. Sun, W. Lu, Z. Li, C. Z. Wang, and K. M. Ho, *J. Chem. Phys.* **129**, 014707 (2008).

⁵¹ W. Zhang, W. Lu, J. Sun, C. Z. Wang, and K. M. Ho, *Chem. Phys. Lett.* **455**, 232 (2008).

⁵² J. G. O. Ojwang, R. van Santen, G. J. Kramer, A. C. T. van Duin, and W. A. Goddard III, *J. Chem. Phys.* **129**, 244506 (2008).

⁵³ J. P. Perdew, K. Burke, and M. Ernzerhof, *Phys. Rev. Lett.* **77**, 3865 (1996).

⁵⁴ G. A. Breaux, C. M. Neal, B. Cao, and M. F. Jarrold, *Phys. Rev. Lett.* **94**, 173401 (2005).

⁵⁵ A. K. Starace, C. M. Neal, B. Cao, M. F. Jarrold, A. Aguado, and J. M. López, *J. Chem. Phys.* **129**, 144702 (2008).

⁵⁶ A. K. Starace, C. M. Neal, B. Cao, M. F. Jarrold, A. Aguado, and J. M. López (unpublished).

⁵⁷ B. Cao, A. K. Starace, C. M. Neal, M. F. Jarrold, S. Núñez, J. M. López, and A. Aguado, *J. Chem. Phys.* **129**, 124709 (2008).

⁵⁸ W. Kohn and L. J. Sham, *Phys. Rev.* **140**, A1133 (1965).

⁵⁹ J. M. Soler, E. Artacho, J. D. Gale, A. García, J. Junquera, P. Ordejón, and D. Sánchez-Portal, *J. Phys.: Condens. Matter* **14**, 2745 (2002).

⁶⁰ R. Hamann, M. Schlüter, and C. Chiang, *Phys. Rev. Lett.* **43**, 1494 (1979).

⁶¹ L. Kleinman and D. M. Bylander, *Phys. Rev. Lett.* **48**, 1425 (1982).

⁶² D. J. Henry, A. Varano, and I. Yarovsky, *J. Phys. Chem. A* **112**, 9835 (2008).

⁶³ D. J. Wales, J. P. K. Doye, A. Dullweber, M. P. Hodges, F. Y. Naumkin, F. Calvo, J. Hernández-Rojas, and T. F. Middleton, The Cambridge Cluster Database (<http://www-wales.ch.cam.ac.uk/CCD.html>).

⁶⁴ L. O. Paz-Borbón, R. L. Johnston, G. Barcaro, and A. Fortunelli, *J. Chem. Phys.* **128**, 134517 (2008).

⁶⁵ M. Lei, K. Maijer, B. von Issendorff, and A. Aguado (unpublished).

⁶⁶ Web page of the “Nanometric Properties of Matter” Research Group (<http://metodos.fam.cie.uva.es/GIR>).

⁶⁷ M. F. Jarrold and V. A. Constant, *Phys. Rev. Lett.* **67**, 2994 (1991).

⁶⁸ A. Aguado, A. Ayuela, J. M. López, and J. A. Alonso, *Phys. Rev. B* **58**, 9972 (1998).

⁶⁹ A. Aguado, F. López-Gejo, and J. M. López, *J. Chem. Phys.* **110**, 4788 (1999).

⁷⁰ M. F. Mesleh, J. M. Hunter, A. A. Shvartsburg, G. C. Schatz, and M. F. Jarrold, *J. Phys. Chem.* **100**, 16082 (1996); **101**, 968 (1997).